

See discussions, stats, and author profiles for this publication at: <https://www.researchgate.net/publication/231650318>

# Base-Directed Formation of Fluorescent Silver Clusters

ARTICLE *in* THE JOURNAL OF PHYSICAL CHEMISTRY C · NOVEMBER 2008

Impact Factor: 4.77 · DOI: 10.1021/jp804031v

---

CITATIONS

111

---

READS

59

6 AUTHORS, INCLUDING:



**Bidisha Sengupta**

Tougaloo College

49 PUBLICATIONS 1,158 CITATIONS

SEE PROFILE



**Peter M Goodwin**

Los Alamos National Laboratory

129 PUBLICATIONS 2,953 CITATIONS

SEE PROFILE

## Base-Directed Formation of Fluorescent Silver Clusters

Bidisha Sengupta,<sup>†</sup> Caroline M. Ritchie,<sup>†</sup> Jenna G. Buckman,<sup>†</sup> Kenneth R. Johnsen,<sup>†</sup> Peter M. Goodwin,<sup>‡</sup> and Jeffrey T. Petty<sup>\*,†</sup>

Department of Chemistry, Furman University, Greenville, South Carolina 29613, and Center for Integrated Nanotechnologies, Mail Stop K771, Los Alamos National Laboratory, Los Alamos, New Mexico 87545

Received: May 7, 2008; Revised Manuscript Received: August 26, 2008

Small silver clusters that form with short oligonucleotides are distinguished by their strong fluorescence. Previous work showed that red- and blue/green-emitting species form with the cytosine oligonucleotide dC<sub>12</sub>. To understand how the bases and base sequence influence cluster formation, the blue/green-emitting clusters that form with the thymine-containing oligonucleotides dT<sub>12</sub>, dT<sub>4</sub>C<sub>4</sub>T<sub>4</sub>, and dC<sub>4</sub>T<sub>4</sub>C<sub>4</sub> are discussed. With dT<sub>12</sub> and dT<sub>4</sub>C<sub>4</sub>T<sub>4</sub>, variations in the solution pH establish that the clusters associate with the N3 of thymine. The small clusters are bound to the larger DNA template, as demonstrated by fluorescence anisotropy, circular dichroism, and fluorescence correlation spectroscopy (FCS) studies. For dT<sub>4</sub>C<sub>4</sub>T<sub>4</sub>, FCS studies showed that approximately 50% of the strands are labeled with the fluorescent clusters. Absorption spectra and the gas dependence of the fluorescence show that nonfluorescent clusters also form following the reduction of the silver cation–oligonucleotide conjugates. Fluorescent cluster formation is favored by oxygen, thus indicating that the DNA-bound clusters are partially oxidized. To elaborate the sequence dependence of cluster formation, dC<sub>4</sub>T<sub>4</sub>C<sub>4</sub> was studied. Cluster formation depends on the oligonucleotide concentration, and higher concentrations favor a red-emitting species. A blue/green emissive species dominates at lower concentrations of dC<sub>4</sub>T<sub>4</sub>C<sub>4</sub>, and it has spectroscopic, physical, and chemical properties that are similar to those of the clusters that form with dT<sub>12</sub> and dT<sub>4</sub>C<sub>4</sub>T<sub>4</sub>. These results suggest that cytosine- and thymine-containing oligonucleotides stabilize a preferred emissive silver cluster.

## Introduction

An important feature of nanomaterials is how the size influences their optical, electronic, magnetic, and chemical properties.<sup>1</sup> Clusters are one general classification of metallic nanomaterials and are comprised of 2–20 atoms with radii less than 0.5 nm.<sup>2</sup> In this size regime, discrete energy levels emerge from the continuous density of states found in larger nanoparticles and bulk metals. This distinction in the energy level organization has a profound impact on the optical properties of metallic clusters, as illustrated by the greatly enhanced radiative decay rates in clusters. For example, a Au<sub>28</sub> species has a fluorescence quantum yield that is over one million times larger than bulk gold.<sup>3,4</sup> Smaller noble metal clusters have even larger fluorescence quantum yields in the range 10%–70%.<sup>5</sup> Additionally, they have high photostabilities and large absorption cross sections, thus making them ideal chromophores.

To inhibit agglomeration, a variety of methods have been used, and these have allowed the unique properties of metallic clusters to be characterized.<sup>6</sup> In solutions, ligands with electron-rich binding sites complex with clusters and stabilize them against further reactions. For example, dendrimers, peptides, and other capping agents have been used for the bottom-up and top-down synthesis of metal clusters.<sup>7–12</sup> Nucleic acids also present nitrogen and oxygen functional groups that coordinate with metallic nanomaterials.<sup>13,14</sup> Nucleic acids are distinguished from other ligands because they can form and stabilize the nanoparticles as well as assemble more complex nanomaterials

via base pairing interactions.<sup>14–16</sup> Our work utilizes DNA as a scaffold for the synthesis of silver clusters composed of 2–10 atoms. Earlier studies were motivated by the sequence specificity of the interaction of silver clusters with cytosine, and recent studies emphasize the key role of this and other bases for the formation of a range of clusters with distinctive fluorescence spectra.<sup>17,18</sup> The present studies consider the role of the bases and the base sequence on the formation of blue/green emitting silver clusters using the oligonucleotides dT<sub>12</sub>, dT<sub>4</sub>C<sub>4</sub>T<sub>4</sub>, and dC<sub>4</sub>T<sub>4</sub>C<sub>4</sub>. The results indicate that both base interactions and inherent cluster stability determine the types of silver clusters that form with DNA.

## Experimental Section

Silver nitrate (204390, Sigma-Aldrich) and sodium borohydride (213462, Sigma-Aldrich) were used as received. The desalted oligonucleotides (Integrated DNA Technologies) were dissolved in deionized water (Elix 10 Water Purification System, Millipore). Buffers with the desired pH contained a total concentration of 5 or 10 mM of the acid/conjugate base. DNA concentrations were determined by absorbance using molar extinction coefficient based on the nearest-neighbor approximation.<sup>19</sup> The silver clusters were synthesized by adding AgNO<sub>3</sub> to the DNA solutions and then adding NaBH<sub>4</sub>, followed by vigorous shaking for 1–2 min. The solutions were kept in the dark prior to the spectroscopic measurements. Absorption (Cary 50, Varian), fluorescence (Fluoromax 3, HORIBA Jobin Yvon), and circular dichroism (J-710, Jasco) spectra were acquired using quartz cuvettes with 1 cm pathlengths. In the case of dT<sub>4</sub>C<sub>4</sub>T<sub>4</sub>, the prominent band in the excitation spectrum has a corresponding absorption band. Thus, the fluorescence quantum yield ( $\Phi_f$ ) for this species was measured using the variation in the

\* To whom correspondence should be addressed. E-mail: jeff.petty@furman.edu.

<sup>†</sup> Furman University.

<sup>‡</sup> Center for Integrated Nanotechnologies, Los Alamos National Laboratory.

fluorescence intensity with the absorbance.<sup>20</sup> Quinine sulfate in 0.05 M H<sub>2</sub>SO<sub>4</sub> ( $\Phi_f = 0.51$ ) was used as the reference chromophore.<sup>21,22</sup> To determine the effect of oxygen and nitrogen on cluster formation, reactions were conducted at 80–100 psi using a high pressure reaction chamber (Parr Instruments).

The fluorescence anisotropy ( $r$ ) values were obtained using the expression

$$r = \frac{I_{VV} - GI_{VH}}{I_{VV} + 2GI_{VH}} \quad (1)$$

where  $I_{VV}$  and  $I_{VH}$  are the vertically and horizontally polarized emission of the silver clusters, respectively, with vertically polarized excitation and  $G$  is the sensitivity factor of the detection system.<sup>23</sup> Each intensity value used in this expression represents the computer averaged values of ten successive measurements. Background fluorescence and scattered light were removed by using a blank solution. All spectral measurements were carried out at 298 K. SYBR Gold (S-11494, Invitrogen/Molecular Probes) complexes with the oligonucleotides were prepared following the protocol from the manufacturer using  $\lambda_{ex} = 490$  nm and  $\lambda_{em} = 530$  nm. Tetramethylrhodamine in glycerol at 279 K showed a limiting anisotropy of 0.35.<sup>24</sup>

For fluorescence correlation spectroscopy studies, excitation at 362 nm with an average power of  $\sim 30$   $\mu$ W was provided by a frequency-doubled mode-locked Ti:Sapphire laser (MaiTai Broadband, Spectra Physics). A  $60\times 1.2$  NA water immersion microscope objective (UPLAN S APO, Olympus), specifically designed to image water-immersed objects up to 200  $\mu$ m away from the coverslip, was used in a laser epi-illuminated geometry to excite the sample and collect the fluorescence emission. A 400-nm long-pass dichroic (Chroma Technology Corporation) reflected the 362-nm excitation into the back of the objective and transmitted the emission. A 75- $\mu$ m diameter pinhole located at the image plane of the microscope tube lens (180 mm focal length) was used to spatially filter the emission collected by the objective. The light transmitted through the pinhole was collimated, and a 500-nm long-pass filter spectrally filtered the emission. A 50% beam splitter split the filtered emission between two actively quenched single-photon counting avalanche photodiode (APD) detectors (SPCM-AQR14, Perkin-Elmer). The APD detector outputs were cross-correlated using a hardware correlator (ALV 5000E/FAST, ALV GmbH). This approach minimized artifacts in the autocorrelation due to detector after pulsing and dead time. Sample droplets were placed on a glass coverslip for analysis. The volume of solvent probed was located  $\sim 25$   $\mu$ m above the coverslip, well within the 200  $\mu$ m working distance of the objective. Because of the highly effective spatial filtering in this setup, background from the coverslip was low. Moreover, spectral discrimination against Raman scattering (385 and 413 nm) and impurity fluorescence was achieved by the large Stokes shift of the DNA/Ag cluster emission. Spectral dispersion of the sample emission confirmed that the fluorescence arises from the clusters. The total background from the borate buffer used for the FCS measurements was 2.5 kHz, which is small compared to the total count rate,  $\sim 100$  kHz, obtained from the DNA/Ag clusters. To confirm that uncorrelated background emission was not significantly influencing the cluster autocorrelation functions, the stock cluster solution with a 10-fold higher concentration was analyzed (data not shown). As expected, the amplitude of the autocorrelation function decreased by approximately a factor of 10 (11 $\times$ ), and the average count rate increased by approximately the same factor (9 $\times$ ).

A dilute solution of the coumarin dye 7-diethylaminocoumarin-3-carboxylic acid (D1421, Invitrogen/Molecular Probes) in water was used as a reference fluorophore to determine the dimensions of the probe volume using a 3-D Gaussian model<sup>25</sup>

$$G(\tau) - 1 = \frac{1}{N} \left(1 + \frac{\tau}{\tau_d}\right)^{-1} \left(1 + \left(\frac{\omega}{z}\right)^2 \left(\frac{\tau}{\tau_d}\right)\right)^{-\frac{1}{2}} \quad (2)$$

where  $G(\tau) - 1$  is the fluorescence autocorrelation,  $\tau$  is the lag time,  $N$  is the average number of fluorescent molecules in the probe volume,  $\omega$  is the transverse radius of the probe volume,  $z$  is the half-length of the probe volume, and  $\tau_d$  is the lag time at which the autocorrelation amplitude has decayed to approximately one-half of its maximum value,  $G(0) - 1$ . The probe volume radius is related to the crossing time and the translational diffusion coefficient ( $D$ ) by

$$\omega = \sqrt{4D\tau_d} \quad (3)$$

The dimensions of the FCS detection volume were determined using the well-established method of fitting the autocorrelation function obtained from a reference fluorophore (coumarin) with a known translational diffusion coefficient.<sup>25</sup> Crossing times,  $\tau_d$ , of 30  $\mu$ s for the coumarin dye were obtained for diffusion in aqueous solution. By use of a coumarin diffusion coefficient of 410  $\mu$ m<sup>2</sup> s<sup>-1</sup> in water, the calculated dimensions of the detection volume are 0.46  $\mu$ m for the diameter ( $2\omega$ ) and 3.7  $\mu$ m for the axial length ( $2z$ ).<sup>26–28</sup> The resulting probe volume ( $\pi^3/2\omega^2z$ ) was 0.54 fL. To validate this volume, the concentration of a reference coumarin solution was measured to be 100 nM via FCS, which compared favorably with the known concentration of 140 nM. A 50-nm band-pass filter centered at 460 nm was used for the measurement of the coumarin autocorrelation.

The silver cluster autocorrelations were fit with the structure factor,  $z/\omega$ , constrained to 8. The average count rate per cluster particle under our excitation conditions ( $\sim 30$  uW average power in a 0.46  $\mu$ m diameter excitation beam giving a time-averaged excitation intensity of  $\sim 20$  kW/cm<sup>2</sup>) is obtained by dividing the total count rate on both APD detectors by the average particle number,  $N$ . From the observed total count rate ( $\sim 130$  kHz) and the average number of clusters in the detection volume obtained from FCS ( $\sim 230$ ), the brightness was in the range of 0.6–0.7 kHz per cluster. The background from the borate buffer solvent under identical excitation conditions was 2.5 kHz. The autocorrelations were collected for 1800 s for the clusters bound to dT<sub>4</sub>C<sub>4</sub>T<sub>4</sub>. The samples were diluted 10-fold in a pH = 10.5 borate buffer. The autocorrelation functions were fit to the 3-D Gaussian model (eq 2) using the Levenberg–Marquardt least-squares minimization algorithm. The autocorrelation data points were weighted in the fit by their standard deviations. The data were collected in 20 runs of 90 s each, and the standard deviations of the averaged autocorrelation data points were directly calculated from the data.

## Results and Discussion

These studies consider how the bases and base sequence determine the types of silver clusters that form with DNA. To preface these observations, prior studies with dC<sub>12</sub> are summarized.<sup>17a</sup> Silver clusters that form with this oligonucleotide are characterized by their red and blue/green emission bands. The most intense emission is red with  $\lambda_{ex} = 580$  nm/ $\lambda_{em} = 650$  nm, and the effect of pH on the intensity of the red emission showed that the clusters bind with the N3 of cytosine. The emission spectra shift with the excitation wavelengths, and this observation suggests that at least two types of red emitting

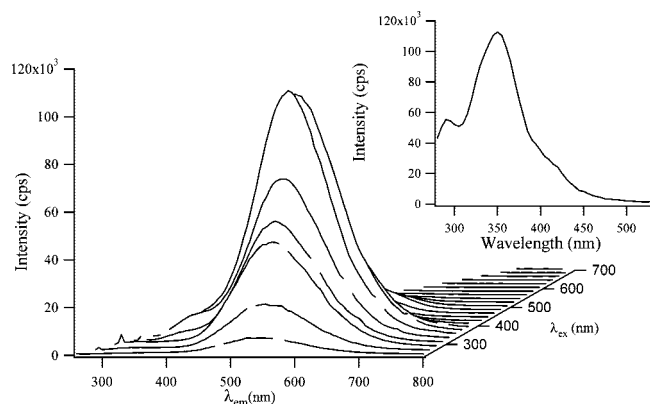


**Figure 1.** A composite fluorescence spectrum of 15  $\mu\text{M}$  dT<sub>12</sub> with 90  $\mu\text{M}$  Ag<sup>+</sup> and 90  $\mu\text{M}$  BH<sub>4</sub><sup>-</sup> in a pH = 10.5 buffer. The emission wavelengths are on the bottom axis, and the excitation wavelengths are incremented by 20 nm on the right axis. The spectra were acquired 16 h after adding BH<sub>4</sub><sup>-</sup>. The inset excitation spectrum was acquired using  $\lambda_{\text{em}} = 540$  nm. The excitation maximum is 350 nm, and weaker transitions are observed at 295 nm and  $\sim 420$  nm.

species form. Over time, the intensity of the red emission diminishes, while the intensity of a transition at  $\lambda_{\text{ex}} = 340$  nm/ $\lambda_{\text{em}} = 495$  nm increases. Through the use of oxidizing and reducing agents, the red emission was attributed to a fully reduced silver clusters, while the blue/green emission was attributed to an oxidized cluster, which is the focus of the present studies.

**Thymine-Rich Oligonucleotides.** When dT<sub>12</sub> is used as the template, green emission is dominant with  $\lambda_{\text{ex}} = 350$  nm/ $\lambda_{\text{em}} = 540$  nm and is stable for several days (Figures 1 and 1S of Supporting Information). The emission depends on pH, and the intensity increases over 100-fold from pH = 8 to 11 with a midpoint at pH  $\approx 9.3$  (Figure 2). The similarity of this midpoint to the  $\text{pK}_{\text{a}} = 9.7$  for the N3 of the thymine base indicates that this deprotonated amine is the binding site for the green emitting cluster.<sup>19</sup> The association of silver clusters with amines is expected, given that electron-rich ligands stabilize metal nanoparticles.<sup>7</sup> Silver cluster formation is favored by close proximity of silver cations on the DNA template, as evident through variations in the relative stoichiometries of silver and DNA. The intensity of the green emission is strongest for a 6 Ag<sup>+</sup>:dT<sub>12</sub> ratio, or 1 Ag<sup>+</sup>:2 bases (Figure 2S of Supporting Information). The increase in intensity from lower stoichiometries suggests that formation of the green emitting cluster is limited by the amount of silver. Comprehensive excitation/emission scans showed that no other emissive species form at lower concentrations, thus suggesting that the green emitting species is the favored cluster size even when the concentrations are below 6Ag<sup>+</sup>:oligonucleotide. At higher stoichiometries, the decreasing fluorescence is attributed to the formation of larger clusters that deplete the number of small, more fluorescent clusters. The formation of other nonemissive clusters is suggested by the absorption spectra (Figure 3). After adding BH<sub>4</sub><sup>-</sup>, the prominent band develops with  $\lambda_{\text{max}} = 430$  nm, and the absorbance of this band diminishes, and the  $\lambda_{\text{max}}$  shifts to longer wavelengths with time. The rates of the decreasing absorbance at 430 nm and of the increasing fluorescence at 540 nm are similar, which suggests that these are distinct species that are linked by a chemical reaction (Figure 4S of Supporting Information). No isosbestic point is observed in the absorption spectra, which suggests that other species contribute to the conversion. With sufficient time, the absorbance in the region 320–360 nm becomes prominent, and this change is ac-

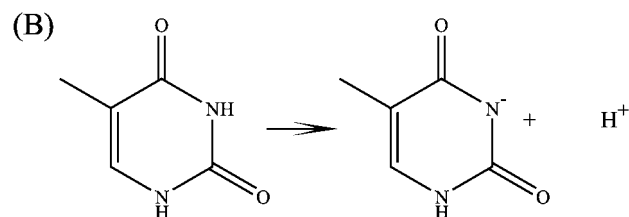
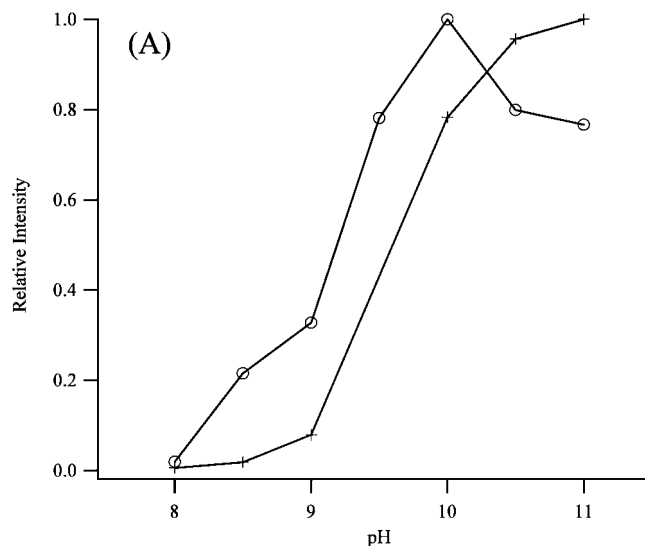


**Figure 2.** (A) Fluorescence intensities of the  $\lambda_{\text{ex}} = 340$  nm/ $\lambda_{\text{em}} = 540$  nm band of dT<sub>12</sub> (open circles) and of the  $\lambda_{\text{ex}} = 360$  nm/ $\lambda_{\text{em}} = 475$  nm band of dT<sub>4</sub>C<sub>4</sub>T<sub>4</sub> (crosses) as a function of pH. The maximum intensities are 150000 cps (dT<sub>12</sub>) and 880000 cps (dT<sub>4</sub>C<sub>4</sub>T<sub>4</sub>). The decreasing fluorescence of the dT<sub>12</sub> samples at higher pH is not dependent on the buffer, as both carbonate and borate buffers demonstrate this behavior. (B) Protonated and deprotonated forms of the N3 of thymine.

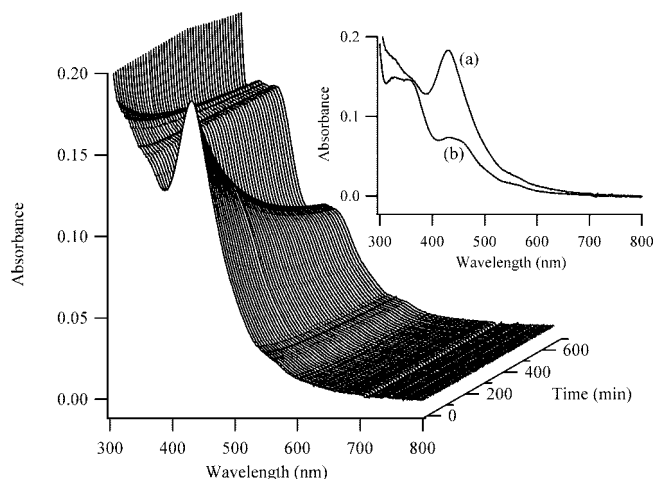


**Figure 3.** Absorption spectra acquired as a function of time (right axis) for the clusters bound to dT<sub>12</sub>. The first spectrum in the series was acquired 2 min after the addition of BH<sub>4</sub><sup>-</sup>, and subsequent spectra were acquired at 7-min intervals. The inset shows the spectra of the clusters acquired at 7 (a) and 700 (b) min after the reaction was initiated.

companied by the development of the fluorescence species with  $\lambda_{\text{ex}} = 350$  nm (Figure 1).

The clusters are bound to the DNA template, as the motion of the clusters is dictated by the oligonucleotide. Steady-state fluorescence anisotropy values are similar for the green emitting silver cluster and for a fluorescent chromophore (SYBR Gold) bound to the same oligonucleotide, which suggests that the motions of the oligonucleotide and the cluster are linked (Table



**TABLE 1: Fluorescence Anisotropies ( $r$ ) of the Silver Clusters**

oligonucleotide	$r$ (cluster–DNA) <sup>d</sup>	$r$ (SYBR gold–DNA)
15 $\mu$ M dT <sub>12</sub> <sup>a</sup>	0.06 $\pm$ 0.01	0.10 $\pm$ 0.02
15 $\mu$ M dT <sub>4</sub> C <sub>4</sub> T <sub>4</sub> <sup>b</sup>	0.14 $\pm$ 0.02	1.12 $\pm$ 0.02
0.5 $\mu$ M dC <sub>4</sub> T <sub>4</sub> C <sub>4</sub> <sup>c</sup>	0.06 $\pm$ 0.01	0.11 $\pm$ 0.01

<sup>a</sup>  $\lambda_{\text{ex}}$  = 350 nm/ $\lambda_{\text{em}}$  = 545 nm, in pH = 10.7 buffer. <sup>b</sup>  $\lambda_{\text{ex}}$  = 370 nm/ $\lambda_{\text{em}}$  = 475 nm, in pH = 10.7 buffer. <sup>c</sup>  $\lambda_{\text{ex}}$  = 340 nm/ $\lambda_{\text{em}}$  = 495 nm, in water. <sup>d</sup> Average of 3–4 measurements.

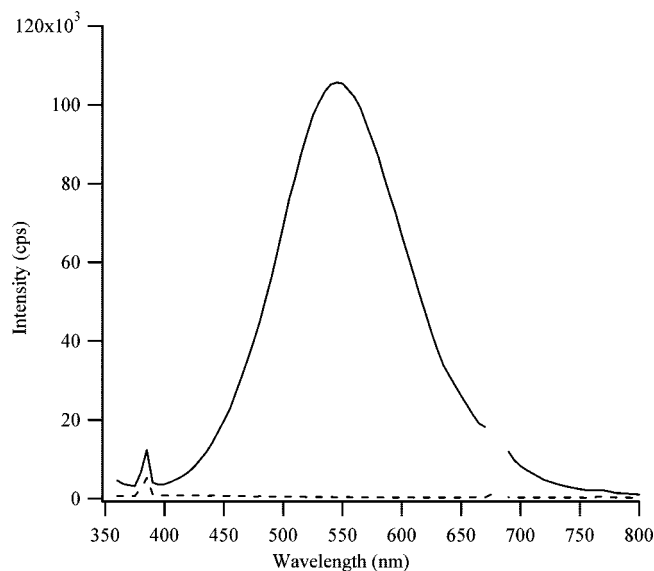


**Figure 4.** Fluorescence spectrum acquired using  $\lambda_{\text{ex}}$  = 340 nm of a 15  $\mu$ M dT<sub>12</sub> with 90  $\mu$ M Ag<sup>+</sup> and 90  $\mu$ M BH<sub>4</sub><sup>−</sup> sample in a pH = 10.5 buffer. The first spectrum (dotted line) was acquired in a solution saturated with N<sub>2</sub>. The second spectrum (solid line) was acquired after O<sub>2</sub> was introduced.

1).<sup>23</sup> Additionally, these anisotropy values are similar to prior measurements of comparably sized oligonucleotides.<sup>29</sup> To provide further support for DNA-templated cluster formation, the electronic transitions in the absorption spectra have corresponding transitions in the circular dichroism spectra (Figure 3S of Supporting Information). Because the small silver clusters are inherently achiral, the induced circular dichroism arises because the clusters are associated with DNA.<sup>30,31</sup>

Further support for the formation of nonfluorescent clusters is provided by the oxygen dependence of the fluorescence. The oxidation/reduction potentials of metal clusters differ from the bulk metal, and our results show that nitrogen and oxygen influence the formation of the dT<sub>12</sub>-bound cluster.<sup>32</sup> With O<sub>2</sub>, the absorption and fluorescence spectra are similar to those obtained in the air-saturated samples (Figures 5S and 6S of Supporting Information). In the presence of N<sub>2</sub>, no emission is observed, but cluster formation is evident based on the formation of colored solutions (Figures 4 and 5S of Supporting Information). To further explore the role of these gases on cluster formation, N<sub>2</sub> and O<sub>2</sub> were used sequentially (Figure 4). The reduction was first conducted in a nitrogen-saturated solution and reacted for 13 h to allow sufficient time for cluster formation. The solution was then saturated with oxygen for 24 h, after which the green emission recovered to a high level comparable to that observed for the air-saturated solutions. Thus, these results indicate that nonfluorescent and reduced clusters form in nitrogen and that oxygen enables the conversion of the nonfluorescent to fluorescent species. Prior studies with dC<sub>12</sub> showed that a reduced red-emitting species converted to an

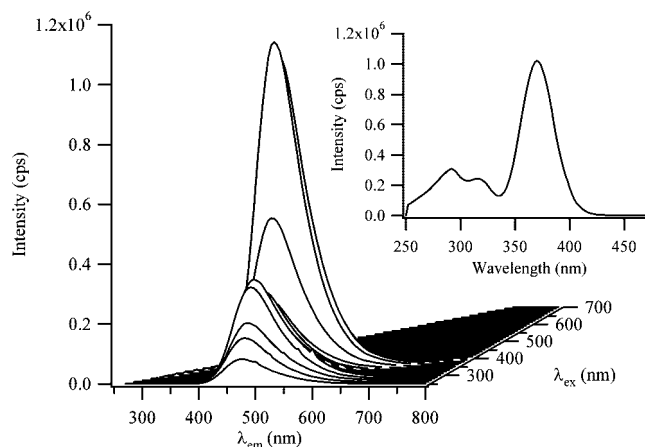


**Figure 5.** A composite fluorescence spectrum of 15  $\mu$ M dT<sub>4</sub>C<sub>4</sub>T<sub>4</sub> with 90  $\mu$ M Ag<sup>+</sup> and 90  $\mu$ M BH<sub>4</sub><sup>−</sup> in a pH = 10.5 buffer. The emission wavelengths are on the bottom axis and the excitation wavelengths are on the right axis. The spectra were acquired 16 h after adding BH<sub>4</sub><sup>−</sup>. The inset excitation spectrum was acquired using  $\lambda_{\text{em}}$  = 475 nm. The excitation maximum is 370 nm, and weaker transitions are observed at 292 and 316 nm.

oxidized blue/green-emitting species.<sup>17a</sup> The absence of red emission with dT<sub>12</sub> suggests that these two types of clusters have different stoichiometries.

The importance of thymine on cluster formation is demonstrated by studies with dT<sub>4</sub>C<sub>4</sub>T<sub>4</sub>. The dominant emission occurs at 475 nm with  $\lambda_{\text{ex}}$  = 370 nm and is stable for several days (Figures 5 and 1S of Supporting Information). In the following respects, the clusters that form with dT<sub>4</sub>C<sub>4</sub>T<sub>4</sub> are similar to those that form with dT<sub>12</sub>. First, the fluorescence intensity increases by over 200-fold as the pH is changed from 8 to 11 (Figure 2). The midpoint of the transition (pH  $\approx$  9.5) is similar to the pK<sub>a</sub> of the N3 of thymine, again demonstrating that this deprotonated amine complexes with the fluorescent silver clusters. Relative to dT<sub>12</sub>, the small shift in the transition may reflect that the base context influences the pK<sub>a</sub> of thymine.<sup>33</sup> Second, fluorescence is suppressed by nitrogen and enhanced by oxygen, which suggests that the fluorescent species is oxidized (Figure 7S of Supporting Information). Third, the silver clusters are bound to the DNA template. The electronic transitions of the clusters have corresponding circular dichroism transitions (Figure 3S). In addition, the fluorescence anisotropy values are comparable for the silver cluster–DNA and SYBR gold–DNA conjugates (Table 1). Fourth, 6 Ag<sup>+</sup>:oligonucleotide stoichiometries yield the maximum fluorescence for both oligonucleotides, which suggests that a favored cluster size is stabilized by both oligonucleotides (Figure 2S of Supporting Information). One notable difference between the two oligonucleotides is that the clusters that form with dT<sub>12</sub> and dT<sub>4</sub>C<sub>4</sub>T<sub>4</sub> have similar excitation maxima in the fluorescence spectra, but the Stokes shift is smaller for the clusters that form with dT<sub>4</sub>C<sub>4</sub>T<sub>4</sub>. This difference suggests that sequence specific interactions influence the environment and hence the spectral properties of the clusters.

Fluorescence correlation spectroscopy provides information about the concentration and the size of the dT<sub>4</sub>C<sub>4</sub>T<sub>4</sub>-cluster conjugate (Figure 6). Because Poisson statistics determine the occupancy of the laser probe, the average number of fluorescent species in the probe volume was determined. By use of the calibrated volume based on the comarin autocorrelation, the concentration of the emitting species was measured to be 7  $\mu$ M, which corresponds to  $\sim$ 50% labeling of the DNA strands. The

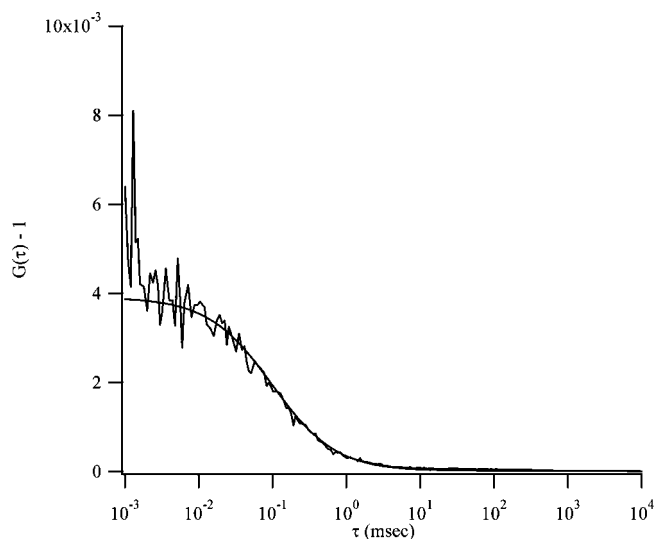


**Figure 6.** Fluorescence autocorrelation function for the clusters attached to dT<sub>4</sub>C<sub>4</sub>T<sub>4</sub>. The smooth line is the weighted fit of the autocorrelation to a 3-D Gaussian model (eq 2). The fit parameters are  $N = 258 \pm 17$  and  $\tau_d = 99 \pm 11 \mu\text{s}$ .

labeling efficiency could be reduced because other less-fluorescent species form, as suggested by the presence of other transitions in the absorption spectra (Figure 3S of Supporting Information). The size of the cluster–DNA conjugate is estimated from the transit times through the focused laser beam. As subsequently discussed, photochemical reactions reduce the transit times at higher laser powers. The lowest average power that provided adequate sensitivity was  $3 \mu\text{W}$ , and the transit time was  $220 \mu\text{s}$ , and the diffusion coefficient is  $240 \mu\text{m}^2 \text{s}^{-1}$ . This value is consistent with the diffusion coefficient measured for a similarly sized thymine oligonucleotide.<sup>34</sup>

The photophysical properties of the blue/green-emitting cluster that forms with dT<sub>4</sub>C<sub>4</sub>T<sub>4</sub> are considered because the absorption band is clearly resolved and the wavelengths of the absorption and fluorescence excitation maxima match. The fluorescence quantum yield for this species is 14%, which is consistent with prior measurements of other small noble metal clusters (Figure 8S of Supporting Information).<sup>5,18</sup> By use of the  $7 \mu\text{M}$  concentration of the clusters from the FCS studies, the extinction coefficient is  $14000 \text{ M}^{-1} \text{ cm}^{-1}$ , which is lower than cluster–DNA conjugates with longer wavelength emission.<sup>18</sup> An estimate of the maximum detection rate, ignoring saturation effects, can be obtained from these spectroscopic parameters and from an estimate of the overall fluorescence detection efficiency. On the basis of an average laser power of  $30 \mu\text{W}$  and a focal radius of  $0.23 \mu\text{m}$ , the emission probability per laser pulse is 0.0014. With an 80-MHz pulse rate and a 5% detection efficiency, the maximum detection rate is 5.6 KHz. The observed detection rate is 0.6–0.7 KHz, and two factors that could compete with radiative decay are considered. First, saturation of the excitation transition would reduce the expected count rate at higher excitation powers. In support, the observed cluster emission intensity is sublinear with respect to the excitation power (Figure 9S of Supporting Information). Second, photoinduced decomposition would reduce the fluorescence. The excitation energy provided by a 362 nm photon is 3.4 eV, which is large compared to the  $\sim 1 \text{ eV}$  bond energy/atom for cationic and neutral silver clusters.<sup>35,36</sup> While DNA is expected to stabilize the cluster, this large difference suggests that photodissociation could be limiting the detection rate. In support, the

FCS transit times decrease from 220 to  $40 \mu\text{s}$  as the average excitation power is increased from 3 to  $170 \mu\text{W}$  (data not shown). Prior studies have noted the lack of photostability of blue emitting clusters.<sup>18</sup>

**Cytosine-Rich Oligonucleotides.** The properties of the clusters that form with the two thymine-rich oligonucleotides are similar, thus suggesting that a common cluster forms with both templates. Prior studies established that an oxidized cluster with blue/green emission also forms with dC<sub>12</sub>. To further explore the sequence dependence of cluster formation, dC<sub>4</sub>T<sub>4</sub>C<sub>4</sub> was used. In contrast with the studies involving dT<sub>12</sub> and dT<sub>4</sub>C<sub>4</sub>T<sub>4</sub>, the concentration of dC<sub>4</sub>T<sub>4</sub>C<sub>4</sub> influences the fluorescence spectra of the clusters. A red emissive species forms with dC<sub>4</sub>T<sub>4</sub>C<sub>4</sub> as also observed with dC<sub>12</sub>, and the emission is dominant at the higher concentration of  $15 \mu\text{M}$  oligonucleotide.<sup>17a</sup> At the lower concentration of  $0.5 \mu\text{M}$ , the only emission band has  $\lambda_{\text{ex}} = 340 \text{ nm}/\lambda_{\text{em}} = 495 \text{ nm}$  (Figure 10S of Supporting Information). The distinct spectra indicate that different species form in these two concentration ranges, and we are currently investigating both concentration and environmental effects on the stoichiometry and spectra of the clusters. In this contribution, we focus on the lower concentrations, as these clusters are most similar to those that form with the other two thymine-rich templates. Besides the spectral similarities, other properties suggest that a common species forms with all the oligonucleotides. First, an oxidized cluster forms with dC<sub>4</sub>T<sub>4</sub>C<sub>4</sub> (Figure 10S of Supporting Information). The fluorescence intensity is suppressed in a nitrogen-saturated solution and subsequently recovers upon exposure to oxygen. Second, the clusters are comprised of a small number of silver atoms, as indicated by the maximum fluorescence at  $8 \text{ Ag}^+:\text{oligonucleotide}$  (Figure 2S of Supporting Information). This stoichiometry is slightly higher than that observed with dT<sub>12</sub> and dT<sub>4</sub>C<sub>4</sub>T<sub>4</sub>, which may be attributed to higher relative  $\text{Ag}^+$  concentrations needed to promote association under these dilute conditions. Third, the fluorescence anisotropy values are similar for the cluster and the SYBR gold, suggesting that both chromophores are attached to a single-stranded DNA template (Table 1). Fourth, the pH dependence of the fluorescence suggests that the bases are involved in stabilizing the clusters (Figure 10S of Supporting Information). The maximum fluorescence occurs at  $\text{pH} \approx 6$ , which is higher than the  $\text{pK}_a$  for the N3 of cytosine. We are currently investigating whether the sequence context could be influencing this pH dependence.

## Conclusions

Two important issues are highlighted by the present and recent studies of silver clusters that form with DNA. First, the bases have a dominant influence on silver cluster formation and stabilization, as the pH dependence of the fluorescence demonstrates that endocyclic amines of the bases are the binding sites of the clusters. Second, specific emissive DNA–silver conjugates are favored, and the present studies consider the blue/green-emitting species forms with dT<sub>12</sub>, dT<sub>4</sub>C<sub>4</sub>T<sub>4</sub>, and dC<sub>4</sub>T<sub>4</sub>C<sub>4</sub>. These cluster–DNA conjugates have similar spectroscopic, physical, and chemical properties, which is consistent with the same species forming with all the oligonucleotide templates. These observations suggest that both base complexation and inherent cluster stability contribute to the types of silver clusters that form with DNA. While the thymine-rich oligonucleotides form only blue/green-emitting species, cytosine-rich oligonucleotides also form red emitting species. We are currently investigating the factors that contribute the sequence dependence of the fluorescence.

**Acknowledgment.** The authors are most appreciative of the comments of the reviewers. J.T.P. gratefully acknowledges the support provided by the National Institutes of Health (R15GM084442 and P20 RR-016461 (from the National Center for Research Resource)), the National Science Foundation (0718588), and the Henry Dreyfus Teacher-Scholar Awards Program. This work was performed, in part, at the Center for Integrated Nanotechnologies, a U.S. Department of Energy, Office of Basic Energy Sciences user facility at Los Alamos National Laboratory (Contract DE-AC52-06NA25396) and Sandia National Laboratories (Contract DE-AC04-94AL85000).

**Supporting Information Available:** Time evolution of the fluorescence emission spectra, dependence of the fluorescence intensity with the relative concentration of  $\text{Ag}^+$ :oligonucleotide for dT<sub>12</sub> (A) and dT<sub>4</sub>C<sub>4</sub>T<sub>4</sub> (B), induced circular dichroism and absorption spectra for the electronic transitions of the cluster–oligonucleotide conjugates, fluorescence intensity of the  $\lambda_{\text{ex}} = 340 \text{ nm}/\lambda_{\text{em}} = 540 \text{ nm}$  fluorescence species and the absorbance (crosses) at 430 nm as a function of time for a sample with 6  $\text{Ag}^+$ :dT<sub>12</sub> in a buffer with pH = 10.5, absorption spectrum of 15  $\mu\text{M}$  dT<sub>12</sub> with 90  $\mu\text{M}$   $\text{Ag}^+$  and 90  $\mu\text{M}$   $\text{BH}_4^-$  in a pH = 10.5 buffer, fluorescence spectrum collected using  $\lambda_{\text{ex}} = 340 \text{ nm}$  for a sample with 15  $\mu\text{M}$  dT<sub>12</sub> with 90  $\mu\text{M}$   $\text{Ag}^+$  and 90  $\mu\text{M}$   $\text{BH}_4^-$  in a pH = 10.5 buffer, fluorescence spectra in solutions saturated with nitrogen and in same nitrogen-saturated solutions that were subsequently saturated with oxygen, fluorescence quantum yield measurements for the cluster–dT<sub>4</sub>C<sub>4</sub>T<sub>4</sub> conjugates, fluorescence emission intensities as a function of the excitation power for a 10 $\times$  diluted sample of 15  $\mu\text{M}$  dT<sub>4</sub>C<sub>4</sub>T<sub>4</sub> with 90  $\mu\text{M}$   $\text{Ag}^+$  and 90  $\mu\text{M}$   $\text{BH}_4^-$  in a pH = 10.5 buffer. This material is available free of charge via the Internet at <http://pubs.acs.org>.

## References and Notes

- (1) Wilcoxon, J. P.; Abrams, B. L. Synthesis, structure and properties of metal nanoclusters. *Chem. Soc. Rev.* **2006**, 35 (11), 1162–1194.
- (2) Kreibitz, U.; Vollmer, M. *Optical Properties of Metal Clusters*; Springer-Verlag: New York, 1995; Vol. 25.
- (3) Link, S.; Beeby, A.; FitzGerald, S.; El-Sayed, M. A.; Schaaff, T. G.; Whetten, R. L. Visible to infrared luminescence from a 28-atom gold cluster. *J. Phys. Chem. B* **2002**, 106 (13), 3410–3415.
- (4) Lee, D.; Donkers, R. L.; Wang, G.; Harper, A. S.; Murray, R. W. Electrochemistry and Optical Absorbance and Luminescence of Molecule-like Au<sub>38</sub> Nanoparticles. *J. Am. Chem. Soc.* **2004**, 126 (19), 6193–6199.
- (5) Zheng, J.; Nicovich, P. R.; Dickson, R. M. Highly Fluorescent Noble-Metal Quantum Dots. *Annu. Rev. Phys. Chem.* **2006**, 58, 409–431.
- (6) (a) Schulze, W.; Rabin, I.; Ertl, G. Formation of Light-Emitting Ag<sub>2</sub> and Ag<sub>3</sub> Species in the Course of Condensation of Ag Atoms with Ar. *Chemphyschem* **2004**, 5 (3), 403–407. (b) Eichelbaum, M.; Rademann, K.; Hoell, A.; Tatchev, D. M.; Weigel, W.; Stöber, R.; Pacchioni, G. Photoluminescence of atomic gold and silver particles in soda-lime silicate glasses. *Nanotechnology* **2008**, 19 (13), 135701. (c) Fierro-Gonzalez, J. C.; Hao, Y.; Gates, B. C. Gold Nanoclusters Entrapped in the  $\alpha$ -Cages of Y Zeolites: Structural Characterization by X-ray Absorption Spectroscopy. *J. Phys. Chem. C* **2007**, 111 (18), 6645–6651.
- (7) Wilcoxon, J. P.; Abrams, B. L. Synthesis, structure and properties of metal nanoclusters. *Chem. Soc. Rev.* **2006**, 35 (11), 1162–1194.
- (8) (a) Crooks, R. M.; Lemon, B. I.; Sun, L.; Yeung, L. K.; Zhao, M. Q. Dendrimer-encapsulated metals and semiconductors: Synthesis, characterization, and applications. *Dendrimers III: Design, Dimension, Function* **2001**, 212, 81–135. (b) Zheng, J.; Dickson, R. M. Individual water-soluble dendrimer-encapsulated silver nanodot fluorescence. *J. Am. Chem. Soc.* **2002**, 124 (47), 13982–13983.
- (9) Yu, J.; Patel, S. A.; Dickson, R. M. In Vitro and Intracellular Production of Peptide-Encapsulated Fluorescent Silver Nanoclusters. *Angew. Chem., Int. Ed.* **2007**, 46 (12), 2028–2030.
- (10) (a) Henglein, A.; Linnert, T.; Mulvaney, P. Reduction of  $\text{Ag}^+$  in Aqueous Polyanion Solution—Some Properties and Reactions of Long-Lived Oligomeric Silver Clusters and Metallic Silver Particles. *Ber. Bunsen-Ges.* **1990**, 94 (12), 1449–1457. (b) Treguer, M.; Rocco, F.; Lelong, G.; Le Nestour, A.; Cardinal, T.; Maali, A.; Lounis, B. Fluorescent silver oligomeric clusters and colloidal particles. *Solid State Sci.* **2005**, 7 (7), 812–818.
- (11) Bertino, M. F.; Sun, Z.-M.; Zhang, R.; Wang, L.-S. Facile Syntheses of Monodisperse Ultrasmall Au Clusters. *J. Phys. Chem. B* **2006**, 110 (43), 21416–21418.
- (12) Duan, H.; Nie, S. Etching Colloidal Gold Nanocrystals with Hyperbranched and Multivalent Polymers: A New Route to Fluorescent and Water-Soluble Atomic Clusters. *J. Am. Chem. Soc.* **2007**, 129 (9), 2412–2413.
- (13) (a) Kryachko, E. S.; Remacle, F. Complexes of DNA Bases and Watson-Crick Base Pairs with Small Neutral Gold Clusters. *J. Phys. Chem. B* **2005**, 109 (48), 22746–22757. (b) Kumar, A.; Mishra, P. C.; Suhai, S. Binding of gold clusters with DNA base pairs: A density functional study of neutral and anionic GC-Au<sub>n</sub> and AT-Au<sub>n</sub> ( $n = 4, 8$ ) complexes. *J. Phys. Chem. A* **2006**, 110 (24), 7719–7727.
- (14) Hinds, S.; Taft, B. J.; Levina, L.; Sukhovatkin, V.; Dooley, C. J.; Roy, M. D.; MacNeil, D. D.; Sargent, E. H.; Kelley, S. O. Nucleotide-Directed Growth of Semiconductor Nanocrystals. *J. Am. Chem. Soc.* **2006**, 128 (1), 64–65.
- (15) Berti, L.; Burley, G. A. Nucleic acid and nucleotide-mediated synthesis of inorganic nanoparticles. *Nat. Nanotechnol.* **2008**, 3 (2), 81–87.
- (16) Liu, D.; Gugliotti, L. A.; Wu, T.; Dolska, M.; Tkachenko, A. G.; Shipton, M. K.; Eaton, B. E.; Feldheim, D. L. RNA-Mediated Synthesis of Palladium Nanoparticles on Au Surfaces. *Langmuir* **2006**, 22 (13), 5862–5866.
- (17) (a) Ritchie, C. M.; Johnsen, K. R.; Kiser, J. R.; Antoku, Y.; Dickson, R. M.; Petty, J. T. Ag Nanocluster Formation Using a Cytosine Oligonucleotide Template. *J. Phys. Chem. C* **2007**, 111 (1), 175–181. (b) Richards, C. I.; Choi, S.; Hsiang, J.-C.; Antoku, Y.; Vosch, T.; Bongiorno, A.; Tzeng, Y.-L.; Dickson, R. M. Oligonucleotide-Stabilized Ag Nanocluster Fluorophores. *J. Am. Chem. Soc.* **2008**, 130 (15), 5038–5039.
- (18) Gwinn, E. G.; O'Neill, P.; Guerrero, A. J.; Bouwmeester, D.; Fyngson, D. K. Sequence-Dependent Fluorescence of DNA-Hosted Silver Nanoclusters. *Adv. Mater.* **2008**, 20 (2), 279–283.
- (19) Bloomfield, V. A.; Crothers, D. M.; Tinoco, I. *Nucleic acids: Structures, properties, and functions*; University Science Books: Sausalito, CA, 2000.
- (20) Williams, A. T. R.; Winfield, S. A.; Miller, J. N. Relative Fluorescence Quantum Yields Using a Computer-Controlled Luminescence Spectrometer. *Analyst* **1983**, 108 (1290), 1067–1071.
- (21) Gelernt, B.; Findeisen, A.; Stein, A.; Poole, J. A. Absolute measurement of the quantum yield of quinine bisulphate. *J. Chem. Soc., Faraday Trans.* **1974**, 2, 939–940.
- (22) Crosby, G. A.; Demas, J. N. Measurement of photoluminescence quantum yields. *J. Phys. Chem.* **1971**, 75 (8), 991–1024.
- (23) Lakowicz, J. R. *Principles of Fluorescence Spectroscopy*; Plenum Press: New York, 1983.
- (24) Burghardt, T. P.; Lyke, J. E.; Ajtai, K. Fluorescence emission and anisotropy from rhodamine dimers. *Biophys. Chem.* **1996**, 59 (1–2), 119–131.
- (25) Rigler, R.; Mets, Ü.; Widengren, J.; Kask, P. Fluorescence Correlation Spectroscopy with High Count Rate and Low-Background-Analysis of Translational Diffusion. *Eur. Biophys. J.* **1993**, 22 (3), 169–175.
- (26) The reported diffusion coefficient for a similar dye, Coumarin 440 (MW: 175.2), in 100% MeOH at 25°C is  $870 \mu\text{m}^2 \text{s}^{-1}$ .<sup>27</sup> This value was corrected for the change in solvent and temperature.<sup>28</sup> The corrected value of the diffusion of the coumarin dye in water is  $410 \mu\text{m}^2 \text{s}^{-1}$ .
- (27) Pappaert, K.; Biesemans, J.; Clicq, D.; Vankrunkelsven, S.; Desmet, G. Measurements of diffusion coefficients in 1-D micro- and nanochannels using shear-driven flows. *Lab on a Chip—Miniaturisation for Chemistry and Biology* **2005**, 5 (10), 1104–1110.
- (28) Wilke, C. R.; Chang, P. Correlation of Diffusion Coefficients in Dilute Solutions. *AIChE J.* **1955**, 1 (2), 264–270.
- (29) (a) Nakamura, M.; Fukunaga, Y.; Sasa, K.; Ohtoshi, Y.; Kanaori, K.; Hayashi, H.; Nakano, H.; Yamana, K. Pyrene is highly emissive when attached to the RNA duplex but not to the DNA duplex: the structural basis of this difference. *Nucleic Acids Res.* **2005**, 33 (18), 5887–5895. (b) Juskowiak, B.; Galezowska, E.; Zawadzka, A.; Gluszyńska, A.; Takenaka, S. Fluorescence anisotropy and FRET studies of G-quadruplex formation in presence of different cations. *Spectrochimica Acta, A* **2006**, 64 (4), 835–843.
- (30) Rodger, A.; Nordén, B. *Circular Dichroism and Linear Dichroism*; Oxford: New York, 1997.
- (31) Shemer, G.; Krichevski, O.; Markovich, G.; Molotsky, T.; Lubitz, I.; Kotlyar, A. B. Chirality of Silver Nanoparticles Synthesized on DNA. *J. Am. Chem. Soc.* **2006**, 128 (34), 11006–11007.
- (32) Henglein, A.; Mulvaney, P.; Linnert, T. Chemistry of Ag<sub>n</sub> aggregates in aqueous-solution-nonmetallic oligomeric clusters and metallic particles. *Faraday Discuss.* **1991**, 92, 31–44.
- (33) Acharya, S.; Barman, J.; Cheruku, P.; Chatterjee, S.; Acharya, P.; Isaksson, J.; Chattopadhyaya, J. Significant pKa Perturbation of Nucleobases

Is an Intrinsic Property of the Sequence Context in DNA and RNA. *J. Am. Chem. Soc.* **2004**, *126* (28), 8674–8681.

(34) Dose, S.; Barsch, H.; Sauer, M. Polymer Properties of Polythymine as Revealed by Translational Diffusion. *Biophys. J.* **2007**, *93* (4), 1224–1234.

(35) Bonacic-Koutecky, V.; Pittner, J.; Boiron, M.; Fantucci, P. An accurate relativistic effective core potential for excited states of Ag atom:

An application for studying the absorption spectra of Ag-*n* and Ag-*n*(+) clusters. *J. Chem. Phys.* **1999**, *110* (8), 3876–3886.

(36) Huber, K. P.; Herzberg, G. *Constants of Diatomic Molecules*; Van Nostrand Reinhold: New York, 1979.

JP804031V